UC Riverside

UC Riverside Previously Published Works

Title

Waves and turbulence in katabatic winds

Permalink

https://escholarship.org/uc/item/4fn137h5

Journal

Environmental Fluid Mechanics, 14(2)

ISSN

1567-7419

Authors

Monti, P
Fernando, HJS
Princevac, M

Publication Date

2014-04-01

DOI

10.1007/s10652-014-9348-1

Peer reviewed

eScholarship.org Powered by the California Digital Library
University of California

Waves and turbulence in katabatic winds

P. Monti, H. J. S. Fernando & M. Princevac

Environmental Fluid Mechanics

ISSN 1567-7419
Volume 14
Number 2

Environ Fluid Mech (2014) 14:431-450
DOI 10.1007/s10652-014-9348-1

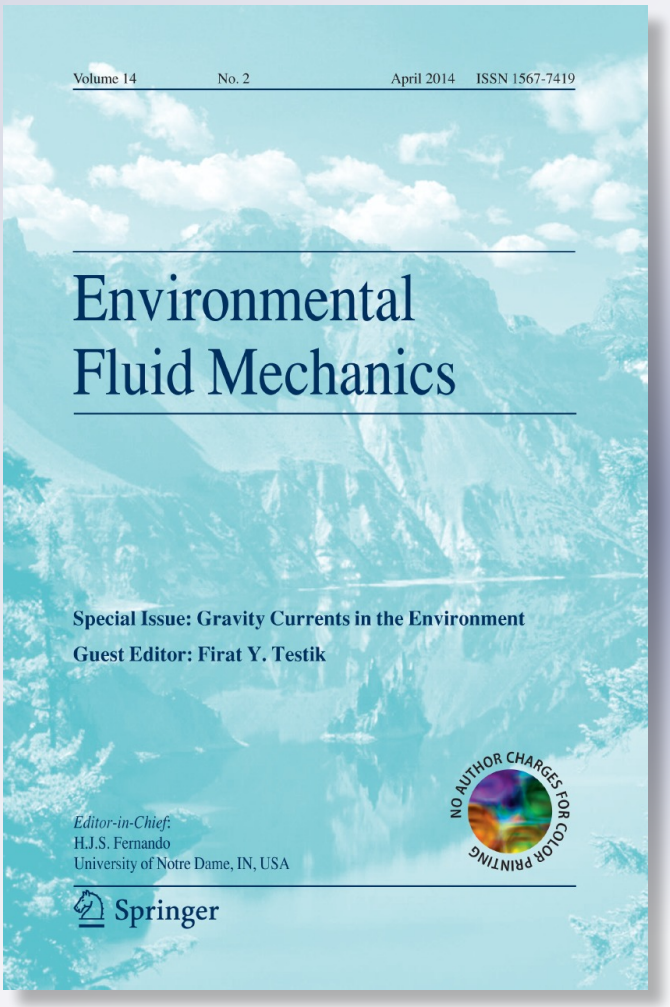

Springer

Your article is protected by copyright and all rights are held exclusively by Springer Science +Business Media Dordrecht. This e-offprint is for personal use only and shall not be self-archived in electronic repositories. If you wish to self-archive your article, please use the accepted manuscript version for posting on your own website. You may further deposit the accepted manuscript version in any repository, provided it is only made publicly available 12 months after official publication or later and provided acknowledgement is given to the original source of publication and a link is inserted to the published article on Springer's website. The link must be accompanied by the following text: "The final publication is available at link.springer.com".

Author's personal copy

Environ Fluid Mech (2014) 14:431–450
DOI 10.1007/s10652-014-9348-1

ORIGINAL ARTICLE

Waves and turbulence in katabatic winds

P. Monti · H. J. S. Fernando · M. Princevac

Received: 25 February 2013 / Accepted: 20 February 2014 / Published online: 5 March 2014
© Springer Science+Business Media Dordrecht 2014

Abstract The measurements taken during the Vertical Transport and Mixing Experiment (VTMX, October, 2000) on a northeastern slope of Salt Lake Valley, Utah, were used to calculate the statistics of velocity fluctuations in a katabatic gravity current in the absence of synoptic forcing. The data from ultrasonic anemometer-thermometers placed at elevations 4.5 and 13.9 m were used. The contributions of small-scale turbulence and waves were isolated by applying a high-pass digital (Elliptical) filter, whereupon the filtered quantities were identified as small-scale turbulence and the rest as internal gravity waves. Internal waves were found to play a role not only at canonical large gradient Richardson numbers ($\overline{\mathrm{Ri_g}} > 1$), but sometimes at smaller values ($0.1 < \overline{\mathrm{Ri_g}} < 1$), in contrast to typical observations in flat-terrain stable boundary layers. This may be attributed, at least partly, to (critical) internal waves on the slope, identified by Princevac et al. [1], which degenerate into turbulence and help maintain an active internal wave field. The applicability of both Monin-Obukhov (MO) similarity theory and local scaling to filtered and unfiltered data was tested by analyzing *rms* velocity fluctuations as a function of the stability parameter z/L, where L is the Obukhov length and z the height above the ground. For weaker stabilities, z/L < 1, the MO similarity and local scaling were valid for both filtered and unfiltered data. Conversely, when z/L > 1, the use of both scaling types is questionable, although filtered data showed a tendency to follow local scaling. A relationship between z/L and $\overline{\mathrm{Ri_g}}$ was identified. Eddy diffusivities of momentum $\mathrm{K_M}$ and heat $\mathrm{K_H}$ were dependent on wave activities, notably when $\overline{\mathrm{Ri_g}} > 1$. The

P. Monti (✉)
Dipartimento di Ingegneria Civile, Edile e Ambientale, Università degli Studi di Roma "La Sapienza", Via Eudossiana 18, 00184 Rome, Italia
e-mail: paolo.monti@uniroma1.it

H. J. S. Fernando
Department of Civil and Environmental Engineering and Earth Sciences, The University of Notre Dame, Notre Dame, IN 46556, USA

M. Princevac
Department of Mechanical Engineering, University of California, Riverside, CA 92521, USA

Author's personal copy

ratio K_H/K_M dropped well below unity at high $\overline{Ri_g}$, in consonance with previous laboratory stratified shear layer measurements as well as other field observations.

Keywords Katabatic winds · Mixing · Stratified flows · MOST · Eddy diffusivity

1 Introduction

Slope flows are ubiquitous in complex terrain, and they are driven by horizontal thermal inhomogeneities resulting from the diurnal heating and cooling of a slope. During daytime, the flow is upslope (anabatic wind) and switches to downslope during the night (katabatic wind), the latter being a special class of gravity currents driven by radiative cooling. During the last several decades, considerable effort has been devoted for determining the dynamics of downslope flows, considering their influence on cloud and fog formation as well as dispersion of contaminants (for reviews, see [2] and [3]).

Research over the past seventy five years has covered a broad class of thermal flows in the atmospheric boundary layer (ABL). Flows in nocturnal ABL with and without complex topography are two simple cases that might shed light on phenomena intrinsic to terrain; the differences and similarities between the two have been striking (e.g. [4–8]). For example, the measurements over sloping ice surfaces [9] show that the stability function ϕ_m (i.e., the non-dimensional wind shear) in the stable boundary layer (SBL) over sloping terrain is rather different from that of flat terrain [10,11], the difference being attributed to the wind maximum observed very close to the ground. Thus, the application of similarity theories for katabatic flows must be considered with circumspection, particularly when the stratification is very strong and other length scales become important.

Another issue of interest is the role of large-amplitude internal waves in katabatic flows. Some previous studies [1,7,12,13] suggest that wave-like non-turbulent motions impair the performances of similarity theory, as they artificially increase the computed scaled variances. This is particularly acute at energetic strongly stratified conditions, especially in katabatic flows, which are known to sustain intense wave activity intermingled with strong shear, instabilities and turbulent motions [1,14]. Princevac et al. [1] reckoned that katabatic flows are associated with along-slope internal wave oscillations, and remarkably, such waves are also critical internal waves that continuously breakdown to turbulence [15]. This is possibly a reason why SBL in complex terrain is in a weakly turbulent state, compared to SBL in flat terrain that tends to be intermittently turbulent. As such, the role of large amplitude internal waves in katabatic flows is more pronounced, and as pointed out in the classic paper by Bretherton [16], waves and turbulence may interact nonlinearly to form an energy cascade. While turbulence is an efficient mechanism for transporting momentum and heat, linear or weakly non-linear waves can transport momentum but not heat or scalars. All these provide impetus for detailed studies of internal waves and turbulence in stable boundary layers of complex terrain.

Under weakly stratified conditions, the heat is carried by turbulent eddies at the same rate as momentum, but when the stratification is strong the propensity for internal gravity waves increases. A challenge is to separate the contributions of these waves from turbulence, so that the fluxes with and without low-frequency (wave) motions can be quantified. This separation is also useful for evaluating similarity theory against data, in cases where only small-scale turbulent motions are to be considered [17,18]. Van der Avoird and Duynkerke [9] calculated fluxes of heat and momentum by using *ogives*, where the *ogive* of frequency f_0 represents the total energy contribution of all frequencies greater than f_0. Mahrt et al. [18]

Author's personal copy

proposed the so called *gap approach*, where perturbation quantities are computed using a small cut-off wavelength whereas a larger cut-off wavelength is used to compute the mean flow and averaged fluxes.

In this paper, an analysis of katabatic flows based on measurements taken at the Vertical Transport and Mixing Experiment (VTMX) is given. A brief description of the site and instrumentation is reported in Sect. 2. Then, an attempt is made to remove low-frequency perturbations by assuming that transport therein occurs through internal waves. In other words, by applying a high pass filter the wave contribution is mostly removed while retaining those of turbulent eddies. The data filtering is described in Sect. 3. Salient parameters such as the friction velocity, turbulent kinetic energy (TKE) and standard deviations (*rms*) of the three wind velocity components are computed with and without filtering, and the results are presented in Sect. 4. Comparisons against the MO similarity theory, stability measures, momentum and heat fluxes as well as eddy diffusivities are presented in this section. Conclusions are given in Sect. 5.

2 Observation site and data description

The data were collected at the north-easterly part of the Salt Lake Valley, Utah, during the October 2000 VTMX field experiment; details on the VTMX program can be found in [19]. The valley, located at $\sim$ 1400 m above the mean sea level (MSL), is approximately 30 km wide along the east-west direction, 50 km long in north-south transect, and is surrounded by elevated mountains up to 3000 m above the MSL. The northwesterly border of the valley coincides with the southern shoreline of the Great Salt Lake. The observation site is a grassy area with a slope of 0.07. The closest uphill feature (nearly 150 m from the measurement station) was the Utah National Guard's Building (10 m high), but it was not in the direct downslope flow path through the station. Although the 1:100 ratio required for the flow to be adjusted to the local surface was not fully satisfied, the uphill features were quite sparse and low in height. Thus, their effect on the flow field at the meteorological station may be considered insignificant. Estimates show that the urban heat island produced by salt lake city metropolitan area and the breeze circulation associated with the lake do not significantly influence nocturnal winds at the measurement site. In addition, the flow is assumed to be (spatially) developing slowly in the downslope direction and the topographic maps show that cross-slope variation is small. Therefore, in dealing with scales of 1 km or smaller, the katabatic flow can be considered as (quasi) one dimensional; also see Princevac et al. [1] for a scaling analysis. With regard to flow unsteadiness, the major unsteady motions arise due to gradual cooling that accelerates the flow (time scales of order hours), critical internal waves that slosh the downslope flow (period $\sim$ 1 h; see [1,14]) as well as a small-scale turbulence and internal waves ($\sim$ minutes) embedded in the flow. The last is the focus of this paper.

The meteorological equipment consists of a 14 m tower instrumented with two ultrasonic fast response (10 Hz sampling rate) anemometer-thermometers placed at 4.5 m (Applied Technologies, Inc.) and 13.9 m (Metek Gmbh) above the ground level (agl) (resolution: wind speed 0.01 ms^{-1}, temperature 0.01 °C). In addition, two cup anemometers (Met One Instruments, Inc.) mounted at 2.0 and 7.3 m agl, two thermistors at 1.8 and 6.9 m, and sensors measuring downward and upward radiation at 3.0 m (Eppley Precision) were part of the instrumentation package. The ultrasonic anemometer wind and temperature data taken at 10 Hz and 5 m averaged data of solar radiation were stored in a data logger. Further details on the site and instrumentation can be found in [14].

Author's personal copy

The field campaign covered 1-18 October 2000, which was characterized by several days of mild meteorological conditions (i.e. clear skies and light synoptic winds) conducive for slope flows. Nocturnal data between 19:00-07:00 local standard time (LST) taken during October 1-October 5 and October 15-October 17 were used for the analysis.

3 Data analysis

In order to separate turbulence from waves, three digital filters were considered: a Butterworth filter, a Bessel filter and an Elliptical filter. Both Butterworth and Bessel filters show nearly flat pass-band characteristics, but their transition band is wide and not smooth. Since a wide transition band precludes a precise cut-off frequency, these filters were not well suited for computation of pure turbulent fluctuations. On the other hand, the Elliptical filter (also known as a Cauer response) seemed to give better performance for our analysis because of its steeper transition band and well-defined cut-off frequency, although it is liable to introduce certain noise in both pass- and stop-bands.

Since propagating internal gravity waves cannot accept frequencies above the buoyancy (or Brünt-Väisälä) frequency,

$$\mathrm{N}^2 = \frac{\mathrm{g}}{\bar{\theta}_r}\frac{\mathrm{d}\bar{\theta}}{\mathrm{dz}}, \tag{1}$$

where $\bar{\theta}_r$ is the mean reference potential temperature, g the gravitational acceleration and z the coordinate aligned with gravity, it could be used as the cut-off for internal waves. The observed N for the analysis period was typically in the range 0.05–0.1 rad s^{-1} (here, $\bar{\theta}_r = [\bar{\theta}_{z=4.5m} + \bar{\theta}_{z=13.9m}]/2$) which corresponds to periods of approximately 1–2 min. Therefore, it was decided to filter out all oscillations with periods exceeding 1 min. By removing slow oscillations, not only the waves are removed but larger turbulent eddies are removed as well; these eddies, however, are buoyancy affected, and sometimes considered as highly non-linear internal waves–that is, high amplitude, quasi periodic buoyancy affected motions that transfers energy between different frequencies and wave numbers [16,20–23]. To investigate the influence of different scales, calculations are made with several cut-off frequencies spanning the range 1–15 min.

The next parameter to be selected was the filter order. Increasing the filter order increases its selectivity but, it simultaneously introduces more noise or unwanted signal components close the band edge [24]. After experimenting with filter orders from one to six, an order-three filter was selected as the most optimal for both velocity and temperature data.

Sample averaging was done over one, five and fifteen minutes, and the mean value was subtracted from the instantaneous signal. This remaining fluctuating component is filtered, leaving only the fluctuations with frequencies higher than the cut-off frequency (*quasi wave-less signal*); they were considered as *pure turbulent fluctuations*, and were used to compute statistics of measured quantities. An example of the time series of a recorded signal (black line) and the third order Elliptic filter (blue line) is presented in Fig. 1.

In what follows, signals are averaged over intervals of stability that are expressed in terms of the mean gradient Richardson number $\overline{\mathrm{Ri_g}}$ (bin averaged), viz.,

$$\overline{\mathrm{Ri_g}} = \frac{\mathrm{N}^2}{\left(\frac{\partial\overline{\mathrm{U}}}{\partial\hat{\mathrm{z}}}\right)^2 + \left(\frac{\partial\overline{\mathrm{V}}}{\partial\hat{\mathrm{z}}}\right)^2}, \tag{2}$$

Author's personal copy

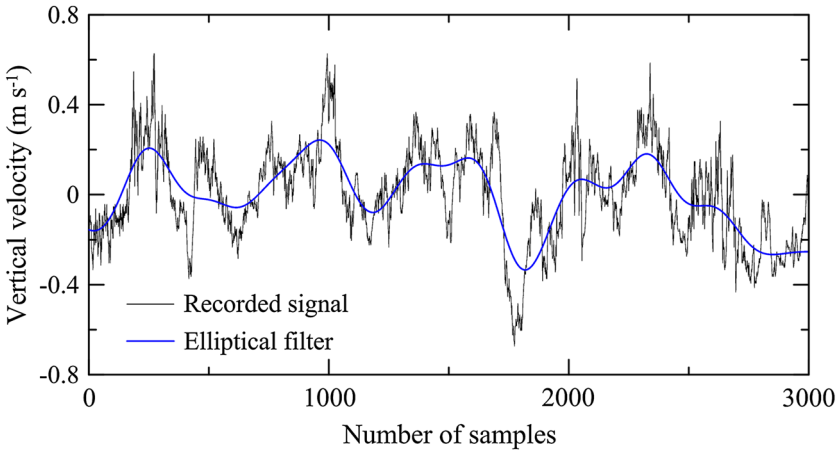

Fig. 1 Five minutes of vertical velocity sampled at 10 Hz after the removal of mean (*black line*). *Blue line* presents elliptical filter of *third* order with *one* minute cut-off period

where $\overline{U}$ and $\overline{V}$ are the mean velocities in a plane parallel to the slope ($\overline{U}$ being the along-slope component, *assumed positive when upslope,* $\overline{V}$ is perpendicular to $\overline{U}$; $\hat{z}$ is the coordinate normal to the slope). In the analysis dealing with MO similarity theory, relevant quantities will be analyzed as a function of the stability parameter z/L, where,

$$L = -\frac{u_*^3 \overline{\theta}}{kg\ \overline{w_z' \theta'}\Big|_s}, \tag{3}$$

is the Obukhov length, $\overline{\theta}$ the mean potential temperature, θ' the potential temperature fluctuation, w_z' the velocity fluctuation along z, *positive when directed upward*, $\overline{w_z' \theta'}\Big|_s$ the buoyancy flux calculated at the ground surface, $k = 0.41$ the von Karman constant and u_* the friction velocity given by

$$u_* = \left[\left(\overline{u'w'}\right)^2 + \left(\overline{v'w'}\right)^2\right]^{1/4}, \tag{4}$$

where u' and v' are the along-slope and lateral velocity fluctuation, respectively, and w' is the normal-to-slope velocity fluctuation. Relations (3), (4) and

$$\overline{\theta}_* = -\overline{w_z'\theta'}/u_*, \tag{5}$$

represent, respectively, some of the relevant scales of length, velocity and temperature of the surface layer.

Since averages of variables defined in terms of a quotient can be dominated by a few large values [7], they were computed by dividing the averages of the numerator and denominator instead of averaging their ratio. Relevant relationships showed smaller scatter when the ratio of the averages was used, especially under strong stability conditions. The vertical gradients were computed from finite differencing the ultrasonic anemometers-thermometers data obtained from the heights $z = 4.5$ m and $z = 13.9$ m agl.

To investigate the dependence of averaged quantities on wave motions, the averaging was done over several different time intervals T_A (30 min, 15 min, 5 min and 1 min) for both non-filtered data and filtered data obtained with different filter cut-off periods T_C. In particular,

Author's personal copy

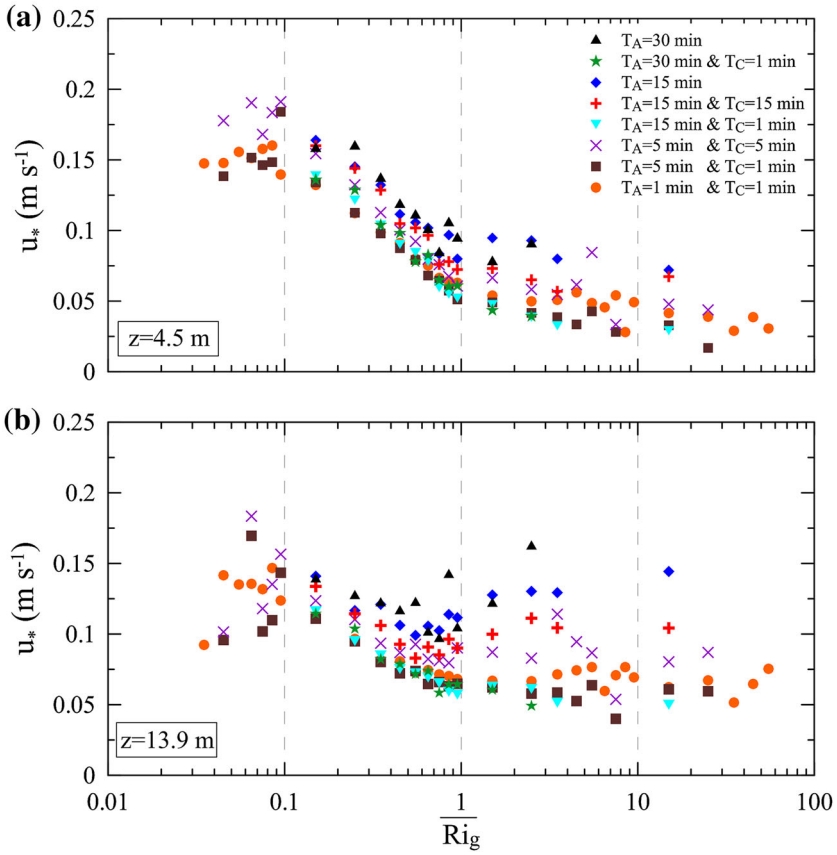

Fig. 2 Friction velocity u_* as a function of $\overline{Ri_g}$ computed at **a** z = 4.5 m and **b** z = 13.9 m

$T_C = 1$ min was selected on the basis of observed N, discussed above, while $T_C = 5$ min and $T_C = 15$ min were used to investigate the effects of T_C. Note that the variety of stability conditions covered using 30 min time segments is limited by relative low number of very weak and very strong stability events contained in the data set.

4 Results

4.1 Friction velocity and turbulent kinetic energy

The friction velocity for z = 4.5 and 13.9 m levels plotted as a function $\overline{Ri_g}$ is given in Figs. 2a and 2b, respectively. The bin size utilized to calculate $\overline{Ri_g}$ is one-tenth the size of the decade in point, while the variables are bin-averaged values. Both panels show an organized dependence of u_* on stability, as well as indications of three stability regimes as proposed by Mahrt et al. [7]. The latter authors, based on the heat flux averaged over the intervals of stability z/L, conjectured the existence of a 'weakly stable regime' for $0 < z/L < \varepsilon << 1$, a 'transition stability regime' for $\varepsilon < z/L < O(1)$, and a 'very stable regime' for $z/L > O(1)$, where ε is the maximum stability for the weakly stable regime (they found $\varepsilon = 0.06$ for observations at 10 m.)

Author's personal copy

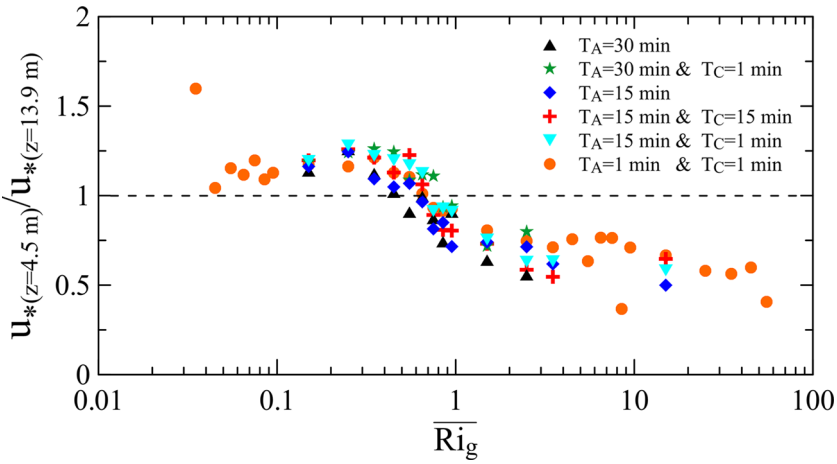

Fig. 3 Ratio of the friction velocity u_* calculated at z = 4.5 m and z = 13.9 m, as a function of $\overline{Ri_g}$

Plots of Fig. 2 are based on the alternative stability measure $\overline{Ri_g}$, from which it is evident that the removal of low frequency wave contributions produces a general lowering of u_* for transition and strong stability regimes. Furthermore, the influence of waves increases with the stability, in agreement with [7] and [9]. The results for filtered data generally converge toward the same value for all the averages performed with $T_C = 1$ min, irrespective of the averaging time T_A. This suggests that the random flux error associated with different T_A used for averaging does not contaminate the results seriously and that, for the filtered data, non-stationarity due to wave-like motions plays a negligible role over the investigated range of $\overline{Ri_g}$. The former contrasts the findings of [7], wherein the random flux errors grew as the record length decreased, in particular for strong stability. This disparity may possibly be due to differing nature of the two data sets. Mahrt et al. [7] analyzed data collected over a flat land, where the very SBL is commonly characterized by weak intermittent turbulence and significant non-stationarity. Conversely, sustained slope winds and degeneration of critical internal waves in our case ensure continuous (though weak) turbulent motions even for strongly stratified conditions [14]; this aspect will be further discussed in Sec. 4.3. In all, $T_C = 1$ min appears to be a sound cut off for the filter.

At z = 4.5 m (Fig. 2a), u_* is nearly constant with $\overline{Ri_g}$ for $\overline{Ri_g} < 0.1$ (weakly stable) while it decreases markedly for $0.1 < \overline{Ri_g} < 1$ (transition regime), irrespective of the values of T_A and T_C. As $\overline{Ri_g}$ further increases ($\overline{Ri_g} > 1$; strong stability regime), u_* continues to decrease at a slower pace than in the transition regime. Figure 2a also shows that in the transition regime the effect of filtering grows with $\overline{Ri_g}$; for example, at $\overline{Ri_g}$=1 the filtered u_* is nearly a factor of 2 lower than the unfiltered u_* for $T_A = 30$ min.

For z = 13.9 m, the data spread and scatter is larger (Fig. 2b), but the three stability regimes are still discernible. Note that in the very stable regime ($\overline{Ri_g} > 1$), in contrast to that at z = 4.5 m, u_* is nearly a constant with $\overline{Ri_g}$, and this holds for both filtered and unfiltered u_*. The results are largely independent on T_A when $T_C = 1$ min.

In the strongly stable regime, quite curiously, u_* associated with pure turbulent fluctuations appears to increase with z, in contrast to typical boundary layer observations (Fig. 3). For example, at $\overline{Ri_g} \cong 10$, the filtered and unfiltered u_* at z = 13.9 m are about 60 % more than that at z = 4.5 m, an increase much higher than the typical 10 % variation accepted in determining the constant flux layer [25]. This implies that canonical MO theory may not

Author's personal copy

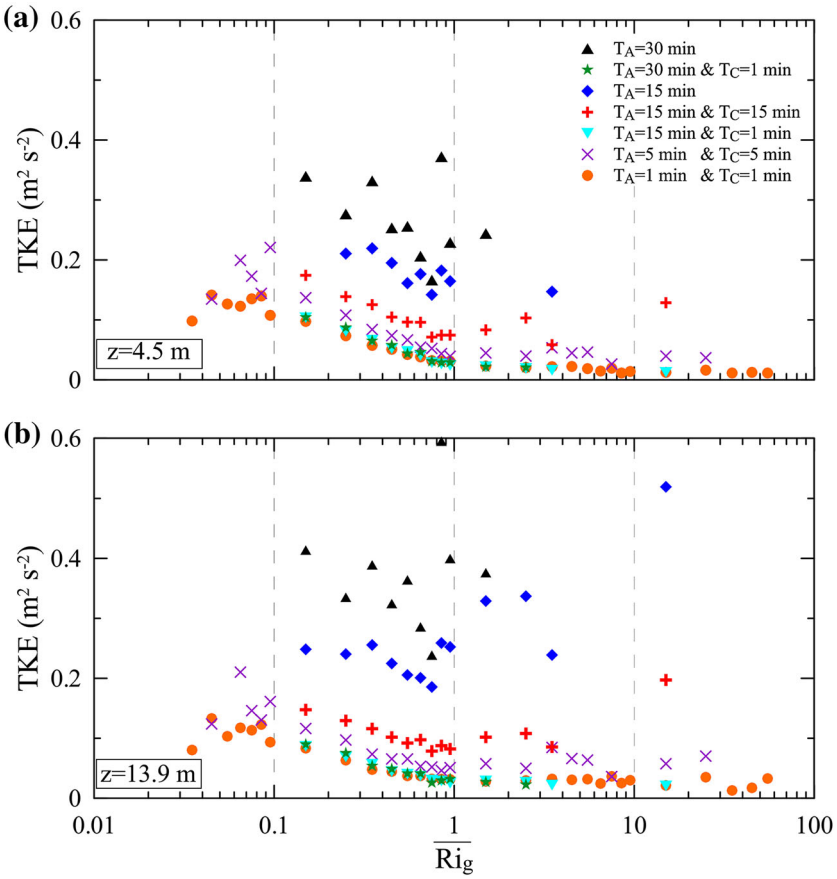

Fig. 4 As in Fig. 2, but for the turbulent kinetic energy TKE. **a** z = 4.5 m and **b** z = 13.9 m

apply for the very stable regime, either when waves and turbulence or only the turbulence is concerned. In contrast, in the transition regime, both unfiltered and filtered signals decrease with z and this lowering, on the average, is about 20 %, which may be marginally acceptable in MO theory applications.

The TKE = $(\overline{u'^2} + \overline{v'^2} + \overline{w'^2})/2$ as a function of $\overline{Ri_g}$ is shown in Fig. 4. There is a resemblance between the TKE and u_* with regard to their contrasting behavior in the three stability regimes. The ratio between the TKE of 'total' motion (unfiltered TKE) and the filtered motions using various T_C show significant wave contributions for transition and highly stable regimes. For example, in terms of percentages, for z = 4.5 m and $\overline{Ri_g} \cong 0.15$, and with $T_A = T_C = 15$ min (red symbols in Fig. 4a), the filtered TKE is about 25 % less than the unfiltered TKE (blue symbols). This becomes ~ 40 % for $T_C = 5$ min and ~ 60 % for $T_C = 1$ min. In other words, for $\overline{Ri_g} \cong 0.15$ and $T_C = 1$, the TKE of pure turbulent fluctuation embodies about 40 % of the total TKE. For stronger stabilities, this is even smaller (~ 15 % at $\overline{Ri_g} \cong 1$). Similar results were obtained for z = 13.9 m (Fig. 4b). Also note that, as for the friction velocity, the TKE for $\overline{Ri_g} > 1$, at z = 4.5 m is somewhat less than that at the upper level.

Author's personal copy

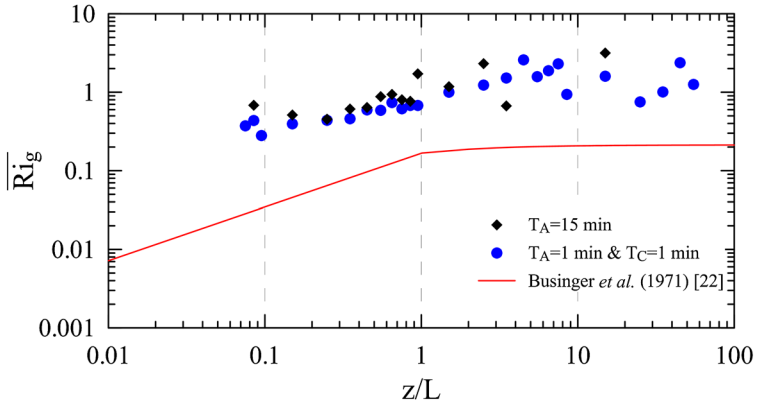

Fig. 5 The dependence of $\overline{Ri_g}$ on z/L at z = 4.5 m (*symbols*). Equation 28 in Businger et al. [26] (*red line*) is also shown

4.2 Scaling of turbulent statistics

In order to verify the applicability of MO similarity theory to the present data set, in this section several non-dimensional quantities are evaluated as a function of z/L. First, we will investigate the relationship between the stability parameters z/L and $\overline{Ri_g}$ Fig. 5 shows $\overline{Ri_g}$ versus z/L (with L based on z = 4.5 m fluxes) for non-filtered (T_A = 15 min, black diamonds) and filtered data (T_A = 1 min and T_C = 1 min, blue circles) as well as the relationships reported in [26] (red line). Although the variations are similar in shape, clear differences exist between the present and past results. This may partly be due to the poor spatial resolution of vertical gradient measurments, a problem frequently encountered in the analysis of near-surface flows under stably stratified conditions. It is interesting that $\overline{Ri_g}$ is quite insensitive to the averaging time (as well as to data filtering, not shown), considering the minor importance of T_A observed in estimating mean quantities for the calculation of $\overline{Ri_g}$.

Figure 6 shows TKE scaled by friction velocity as a function of z/L for z = 4.5 m and for z = 13.9 m; all are based on local quantities, hereinafter referred to as $\left[(TKE/u_*^2)_{4.5\,m}\right]_{L(4.5\,m)}$ (diamonds) and $\left[(TKE/u_*^2)_{13.9\,m}\right]_{L(13.9\,m)}$ (circles), respectively. The 'mixed case' [7] $\left[(TKE/u_*^2)_{4.5m}\right]_{L(13.9m)}$ (triangles) is also shown, where the normalized TKE is based on z = 4.5 m data and L on z = 13.9 m data. For simplicity, only the cases of non-filtered data with T_A = 5 min (full symbols) and filtered data with $T_A = T_C$ = 1 min (open symbols) are given. The plots for non-dimensional *rms* velocities, $\sigma_U = (\overline{u'^2})^{1/2}$, $\sigma_V = (\overline{v'^2})^{1/2}$ and $\sigma_W = (\overline{w'^2})^{1/2}$ scaled with u_*, are presented in Figs. 7a–c.

With regard to the filtered data, Fig. 6 illustrates that for z/L < 1 the three relationships are approximately the same, indicating that TKE/u_*^2 is independent of height. In contrast, for z/L > 1, the mixed case (triangles) departs considerably from the other two that show similar trends. Broadly, the same remarks may apply for the distributions of filtered *rms* (Fig. 7a–c). These observations suggest that, for filtered data, the MO similarity theory and the local scaling apply for TKE reasonably well for both the weak and transition regimes, while the MO or the local scaling is questionable for the very stable regime. The latter points to the global nature of the flow characteristics, possibly introduced as a result of propagating internal waves.

A strong increase of the scaled *rms* has also been reported previously ([12,27] and [28], among others), which is a direct consequence of the rapid decrease of u_* with z/L as a result of

Author's personal copy

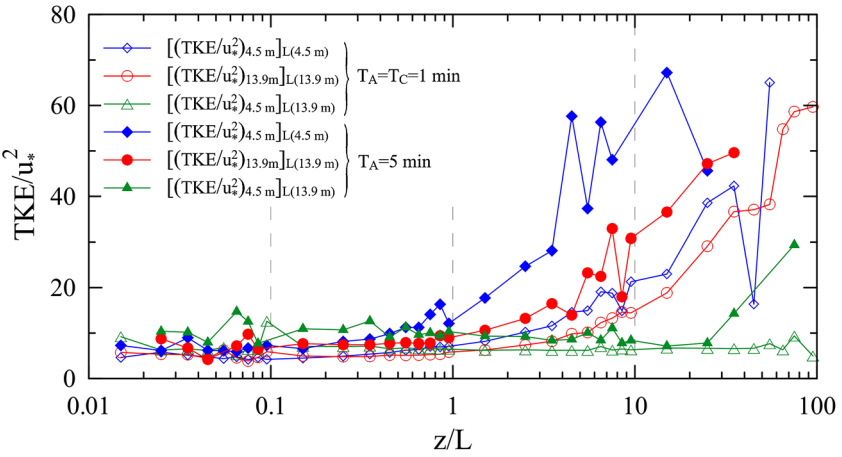

Fig. 6 Non-dimensional TKE as a function of z/L computed with filtered (*open symbols*) and unfiltered (*full symbols*) data for z = 4.5 m, z = 13.9 m and the mixed cases

smaller vertical fluxes with increased stratification. Note that all ratios in Figs. 6 and 7 remain nearly constant for $z/L < 1$, wherein the stratification is weaker and internal-waves influence is less significant. As z/L increases ($z/L > 1$), the internal waves contribute strongly (filtered and unfiltered quantities diverge on the plot), ground influence wanes (u_* varies in the surface layer) and z becomes unimportant as horizontal layers decouple (z-less stratification [27]); all these lead to non-similarity behavior observed in Fig. 7 for $z/L > 1$. Pahlow et al. [28] found $z/L \cong 0.1$ as the limit below which the scaled *rms* values show constancy, whereas much greater range, $z/L < 30$, has been identified during aircraft measurements over Greenland [29]; perhaps additional factors are determining the threshold. Other possible reasons for the failure of MO theory in katabatic winds include horizontal inhomogeneity [10] and hydraulic phenomena [3,30].

Nominally, the dependence of unfiltered quantities on z/L, especially scaled TKE and *rms* horizontal velocity components, has higher variability compared to their filtered counterparts, and this generally holds true over the entire z/L range, albeit the differences are smaller for $z/L < 1$. This agrees well with Van der Avoird [9], although Mahrt et al. [7] noted distinct differences between filtered and non-filtered scaled *rms* for horizontal velocity fluctuations only in the very stable regime. Also note that in the weak and transition regimes the MO similarity allows approximately describing the velocity variances of both filtered and non-filtered data. For the very stable regime, both MO and local scaling do not work well for the filtered and unfiltered σ_U/u_*. In contrast, in the same regime, the local scaling for filtered data works adequately for σ_V/u_*.

The σ_W/u_* (Fig. 7c) follows somewhat distinct behavior compared to its horizontal counterparts. First, as pointed out in [6,7] for flat-terrain boundary layer, large-scale low-frequency motions play a lesser role for σ_W/u_* for all stability conditions, and hence filtered and unfiltered signals are closer. Second, the resemblance between $\left[(\sigma_W/u_*)_{4.5\,\mathrm{m}}\right]_{\mathrm{L}(4.5\,\mathrm{m})}$ and $\left[(\sigma_W/u_*)_{13.9\,\mathrm{m}}\right]_{\mathrm{L}(13.9\,\mathrm{m})}$, the disparity between mixed scaling, and the similarity between filtered and unfiltered signals indicate that for strong stability regime the local scaling is appropriate for σ_W/u_* irrespective of wave motions. The magnitude of all three locally scaled *rms* velocities for the filtered case are comparable over the entire range of stabilities, σ_W/u_* for the strongly stable case is lower, which is in agreement with [28].

Author's personal copy

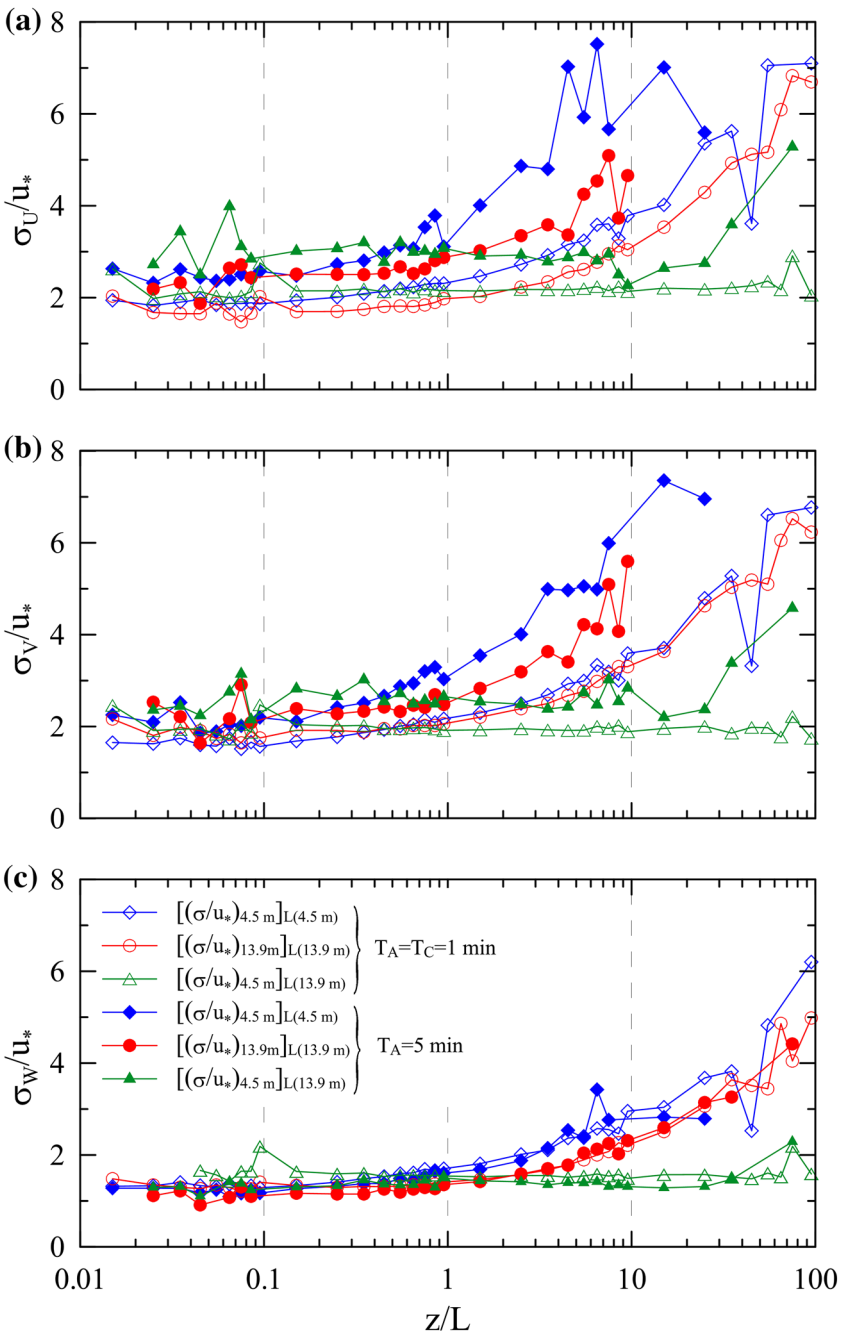

Fig. 7 As in Fig. 6 but for **a** σ_U / u_*, **b** σ_V / u_* and **c** σ_W / u_*

The *rms* temperature fluctuations $\sigma_\theta = \left(\overline{\theta'^2}\right)^{1/2}$ normalized by the temperature scale θ_* as a function of z/L is reported in Fig. 8. Since both σ_θ and $\theta_* \to 0$ as $z/L \to 0$, at very weak stabilities σ_θ / θ_* assumes unphysical large values. This is particularly true for $z = 13.9$ m

Author's personal copy

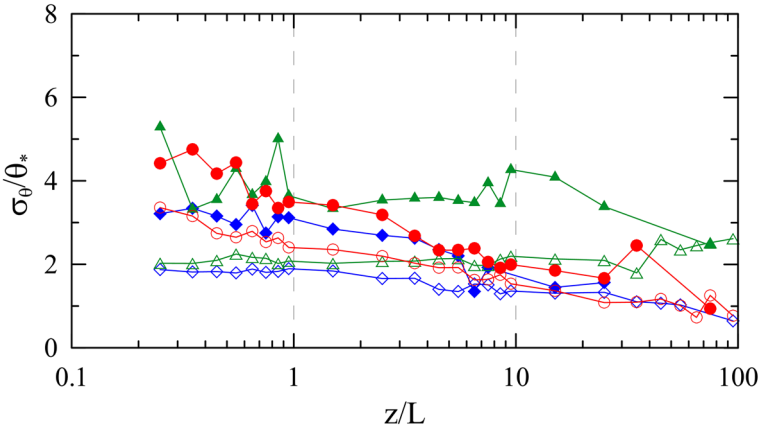

Fig. 8 As in Fig. 6 but for σ_θ/θ_*. The symbols have the same meaning as in Fig. 6

(circles), where the buoyancy flux is subjected to larger measurement errors. As such, Fig. 8 is limited to $z/L \geq 0.2$, but still it is rather difficult to draw clear conclusions. Indications are that the local scaling may be valid for $z/L > 1$, although the data are scattered. Moraes et al. [31] found that the MO similarity applies for σ_θ / θ_* when $z/L < 2$ (the strongest stability of their study) while Mahrt et al. [7] suggests that the validity is restricted to $z/L < 1$.

Unlike in the case of scaled *rms* velocities, σ_θ / θ_* decreases with z/L, irrespective of the height of measurement or filtering. This is at variance with King [6] and Mahrt et al. [7] that reported an increase of σ_θ / θ_* with z/L and with Pahlow et al. [28] where σ_θ / θ_* approached a constant (≈ 3). The results are in partial agreement with Van der Avoird and Duynkerke [9] who reported a decrease of σ_θ / θ_* with z/L for unfiltered data. The reduction may be a consequence of non-negligible buoyancy fluxes observed at large z/L, a signature of strong nonlinear gravity waves that enhances the buoyancy flux and hence θ_*. Princevac et al. [1] noted theoretically, and demonstrated using data, that critical internal waves are prevalent in highly stratified conditions, and their continuous breaking, as illustrated by DeSilva et al. [15], may cause high buoyancy fluxes. Therefore, a clear difference seems to exist between turbulence in katabatic flows and flat terrain nocturnal boundary layers.

4.3 Heat and momentum fluxes

The heat flux $\overline{w'\theta'}$ as a function of $\overline{Ri_g}$ for $z = 4.5$ m and $z = 13.9$ m is plotted in Figs. 9a and 9b, respectively. The three stability regimes are clearly discernible at both levels. For weakly stable regime ($\overline{Ri_g} < 0.1$), the downward (negative) heat flux grows as the Richardson number increases, a result of increasing temperature fluctuations associated with higher temperature gradients. Then, it drops in the transition regime until $\overline{Ri_g} \sim 1$. For $\overline{Ri_g} > 1$, $\overline{w'\theta'}$ continues to decrease very slowly at $z = 4.5$ m, while at z = 13.9 it remains nearly constant. The heat flux remains negative even for large $\overline{Ri_g}$.

The maximum (negative) heat flux occurs at $z/L \sim 0.2$ for $z = 4.5$ m, in agreement with [32] and [28] and at $z/L \sim 0.7$ for $z = 13.9$ m (equivalent to $\overline{Ri_g} \sim 0.1$ in both cases). Mahrt et al. [7] found the maximum heat flux at $z/L \sim 0.02$ for z = 10 m and at $z/L \sim 0.06$ for z = 3 m. They attributed this z/L variation to the decrease of heat flux with height. We find that this variation disappears when $\overline{Ri_g}$ instead of z/L is used (Fig. 9), pointing to the usefulness of $\overline{Ri_g}$ in characterizing stability. The effect of filtering is of lesser importance at $z = 4.5$ m

Author's personal copy

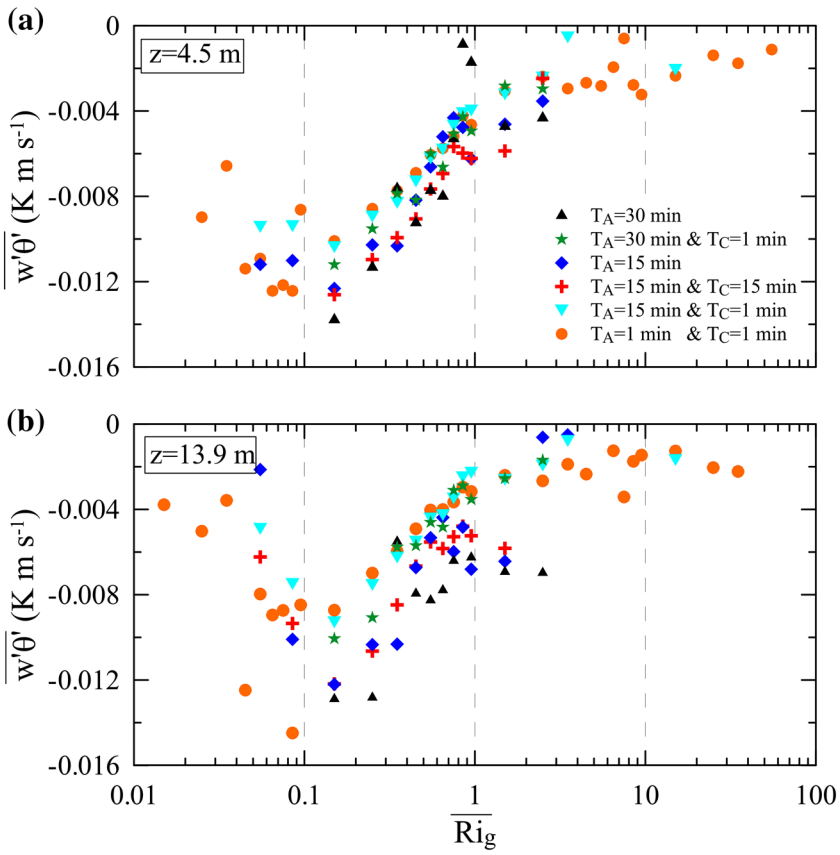

Fig. 9 As in Fig. 2 but for buoyancy flux $\overline{w'\theta'}$

for transition and strong stability regimes, while, with filtering, discernible lowering of $\overline{w'\theta'}$ magnitude occurred at z = 13.9 m, indicating greater internal wave activity at this level, particularly at higher stabilities.

While $\overline{w'\theta'}$ at z = 4.5 m and z = 13.9 m are nearly comparable, the momentum fluxes $\overline{u'w'}$ at the two levels are clearly different. Figure 10 presents the plots for the momentum flux scaled with the square of the local friction velocity $\overline{u'w'}/u_*^2$ as a function of $\overline{Ri_g}$ for the two heights (note that given the negative sign of the along slope velocity, positive $\overline{u'w'}$ refer to downward momentum fluxes and *vice versa*). At z = 4.5 m, $\overline{u'w'}/u_*^2$ is generally positive (Fig. 10a), and this height usually corresponds to that with a negative sign of mean shear [14]; hence the turbulent kinetic energy production is positive.

In contrast, at z = 13.9 m, $\overline{u'w'}/u_*^2$ is positive for the weak and for the transition regimes until $\overline{Ri_g} \cong 0.25$ (Fig. 10b), and then becomes negative. If there is negative shear, this implies that TKE can be transferred to the mean flow, which is plausible in strongly stratified shear flows. Rotter et al. [33] demonstrated, through direct laboratory measurements of turbulence and flow visualization, the possibility of negative shear production in the TKE budget at large $\overline{Ri_g}$, whence the flow is relaminarizing and turbulence becoming extinct. Given the complexity introduced by the stratification, the shear production terms so observed, however, ought to be carefully interpreted.

Author's personal copy

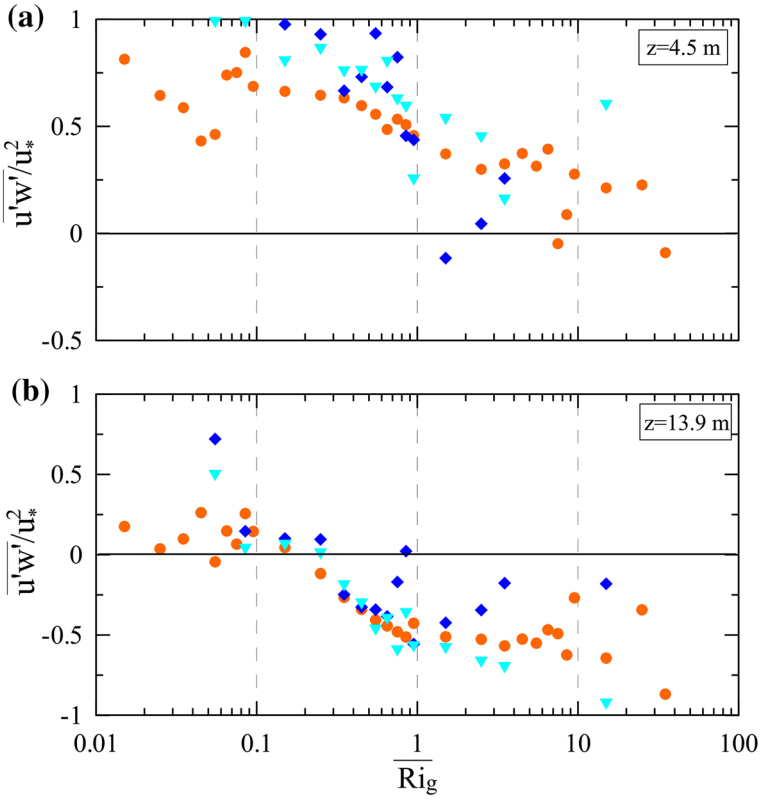

Fig. 10 As in Fig. 9 but for momentum flux $\overline{u'w'}/u_*^2$

To this end, one may cogently argue that poor spatial measurement resolution in the vertical confounded by the occurrence of near-surface jets under strong thermal stratification can be a reason for the above observations. In fact, when the stability is moderate or strong, a large number of events in which the downslope velocity maximum takes place between the two measurement levels, or even below the lower one, occurred. For example, Figs. 11a,b depict the vertical profiles of along slope velocity and temperature obtained from a tethered balloon launched during the early night of 3 October and 15 October, respectively (see [14] for details).

The above further exemplifies the difficulties associated with the computation of near-surface momentum fluxes in SBLs. Also, the existence of very shallow katabatic layers, together with coarse vertical resolutions often used in numerical codes, are clear examples of problems encountered by numerical modelers attempting to simulate atmospheric flow and pollutant dispersion over complex terrain under stably stratified conditions near the surface.

4.4 Eddy diffusivities of heat and momentum

It is well-known that eddy diffusivities of momentum

$$K_M = -\frac{\overline{u'w'}}{\partial \overline{U}/\partial z}, \tag{6}$$

Author's personal copy

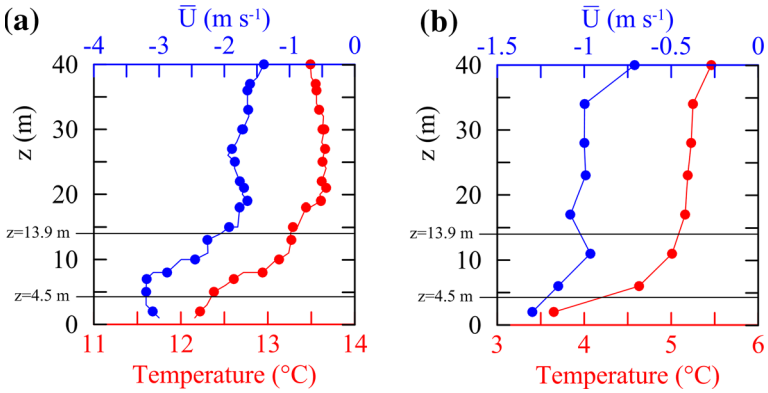

Fig. 11 **a** Vertical profiles of along slope velocity (*blue line*) and temperature (*red line*) obtained from tethered balloon measurements during the night of 3 October (03:34 LST). **b** as in a), but for 15 October 01:01 LST

and heat

$$K_H = -\frac{\overline{w'\theta'}}{\partial\bar{\theta}/\partial z}, \tag{7}$$

play key roles in modeling of geophysical flows. Despite their extensive use, parameterizations of K_M and K_H for stable stratified flows are still being debated, particularly for strongly stratified conditions [14].

Of particular concern in diffusivity calculations are the simultaneous occurrences of either negative or positive mean shear and the vertical flux of horizontal momentum, giving rise to negative (unphysical) eddy diffusivities. Figures 12a,b show K_M as a function of $\overline{Ri_g}$ at $z = 4.5$ m and $z = 13.9$ m, respectively. The instances with negative K_M have been neglected in bin-averaging. Computations of K_H at the two measurement levels, similarly calculated, are shown in Fig. 13. For clarity, only the results referred to $T_A = T_C = 1$ min (filtered data, red circles) and $T_A = 5$min (unfiltered, blue squares) are displayed in the figures.

Both filtered and unfiltered data for z = 4.5 m (Fig. 12a) indicate that K_M is nearly constant with $\overline{Ri_g}$ for the weakly stable regime. Then, it slightly decreases for the transition regime, while slightly increases for the strongly stable regime. Filtered and unfiltered values are similar for all three regimes, indicating the lesser role of internal waves at $z = 4.5$ m. In contrast, at $z = 13.9$ m (Fig. 12b), filtered K_M are lesser than unfiltered K_M, in particular for the transition and the strongly stable regimes.

Our K_M results at $z = 13.9$ m differ much from those presented by Mahrt [11], which show a well-defined reduction of eddy viscosity as z/L increases from the weak stability regime onwards. The differences between Mahrt's [11] and our results in the transition regime can be attributed to possible intense Kelvin-Helmholtz billowing, which can be present when $\overline{Ri_g}$ is in the range 0.2–1 [34,35]. This, however, cannot explain the behavior of K_M in the strong stability regime at the upper measurement level, where an increase of unfiltered and filtered K_M is seen. Continued vertical mixing due to degeneration of large amplitude waves due to (local) internal shear [1] can be a possible cause, but further diagnostics based on high resolution measurements are needed to investigate this aspect. Also, given the small number of events for high $\overline{Ri_g}$ in the time series, data points for $\overline{Ri_g} > 5$ need to be viewed with circumspection.

Author's personal copy

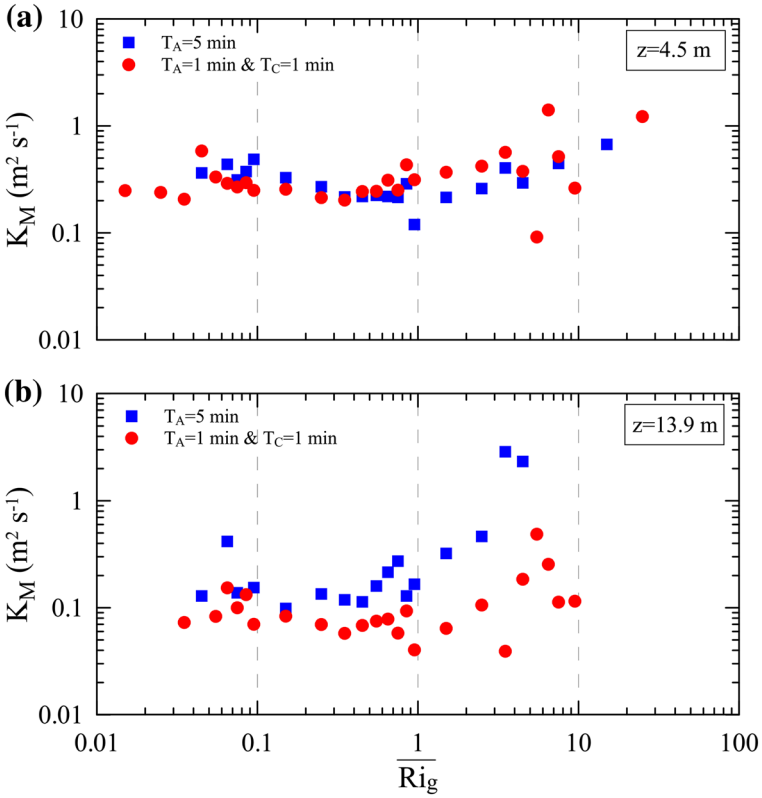

Fig. 12 Eddy diffusivity of momentum K_M as a function of $\overline{Ri_g}$ for unfiltered ($T_A = 5$ min, blue squares) and filtered data ($T_A = T_C = 1$ min; *red circles*) computed for **a** z = 4.5 m and **b** z = 13.9 m

The eddy diffusivity of heat K_H (Fig. 13) follows rather different dynamics in comparison to K_M, in that a marked lowering of K_H with increasing $\overline{Ri_g}$ is seen in the transition regime (nearly one order of magnitude), possibly due to the increasing role of internal gravity waves, which sustain only little buoyancy flux. This is more evident at z = 13.9 m (cf. Figs 12b and 13b), where the internal wave activities are arguably stronger.

The inverse of the turbulent Prandtl number K_H/K_M is presented in Fig. 14 as a function of $\overline{Ri_g}$; it drops markedly at both levels as $\overline{Ri_g}$ increases. This is particularly evident at z = 13.9 m (Fig. 14b), wherein K_H/K_M is lower compared to that at z = 4.5 m for $\overline{Ri_g} > 3$, highlighting the greater role of internal waves at the upper level. Also shown are the parameterizations proposed by Mahrt and Vickers [36] based on field observations, Strang and Fernando [35] based on laboratory water tunnel data and by Monti et al. [37] based on tilting tube data. The agreement among them is reasonable, in particular between [35,36] and the present observations at z = 4.5 m. There are also other data sets that do not show strong dependence of K_H/K_M on stability, wherein K_H/K_M is approximately estimated as unity (e.g., [38] and [29], among others). Again, this disagreement, in part, may be a consequence of the type of terrain; flat terrain versus a mountain slope in the present work. Also, the lower K_M in the low stability regime compared to K_H is an artifact of data processing and measurement uncertainties as discussed below.

Finally, a question arises regarding $d\overline{U}/dz$ and $d\overline{\theta}/dz$ values used in the calculation of the eddy diffusivities. We acknowledge that the use of velocity gradients based on the differences

Author's personal copy

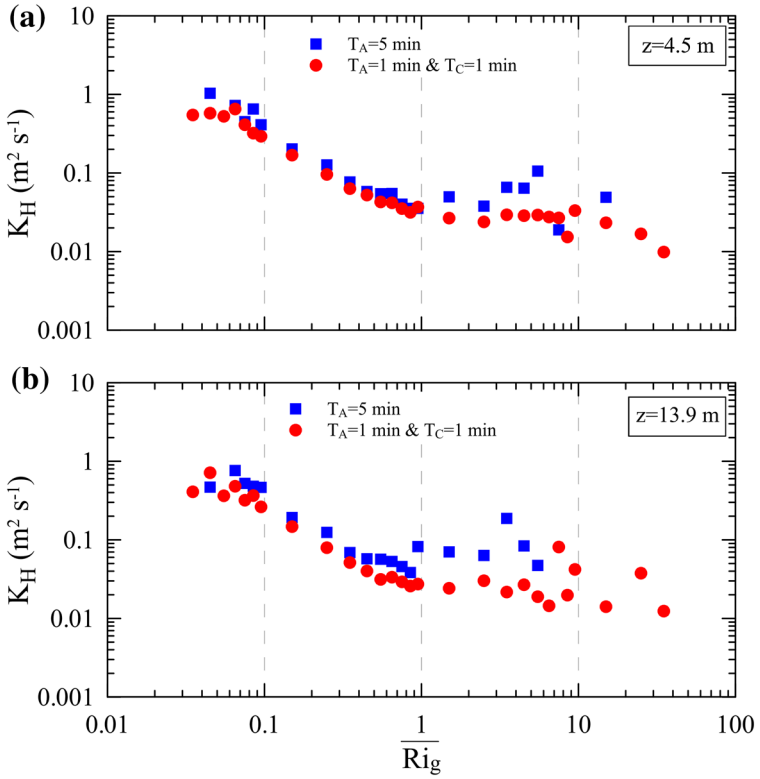

Fig. 13 As in Fig. 12 but for the eddy diffusivity of heat K_H

between z = 4.5 m and z = 13.9 m to compute K_M and K_H is not entirely justified, and very likely the mean shear at z = 4.5 m is greater. As a consequence, K_M at z = 4.5 m might be overestimated. On the other hand, since the surface imposes less stringent conditions for temperature rather than for velocity, it is plausible that errors in $d\overline{\theta}/dz$ for z = 4.5 m are lesser compared to that of $d\overline{U}/dz$. In addition, under the near-neutral conditions the difficulty of estimating very small temperature gradients may result in an underestimation of $d\overline{\theta}/dz$. These issues may explain $K_H/K_M > 1$ values computed for the weak stability regime at both measurement levels.

5 Summary and conclusions

Nocturnal field observations taken during the VTMX (Vertical Transport and Mixing) Experiment conducted in Salt Lake Valley, Utah, during October 2000, were analyzed to study the statistics of turbulent fluctuations in downslope winds over a gentle slope ($\sim$ 0.07). The data obtained from two ultrasonic anemometer-thermometers operating at 10 Hz, placed at z = 4.5 m and z = 13.9 m agl, were used. The study considered nine nights, corresponding to periods of clear skies and low synoptic winds, dominated by thermal circulation.

The effects of low frequency internal waves were investigated by removing them via a high-pass Elliptical filter, with a cut-off period $T_C = N^{-1} = 1$min, N being the buoyancy frequency. The statistics based on filtered data were considered as those of pure (three-

Author's personal copy

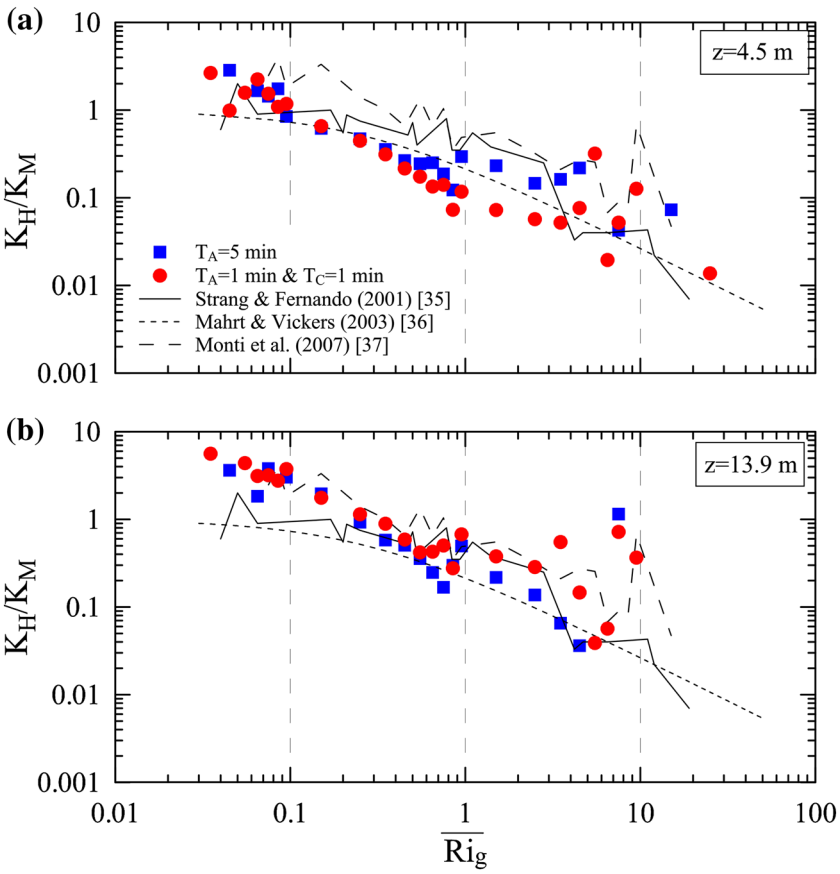

Fig. 14 As in Fig. 12 but for the ratio K_H/K_M. The laboratory data of [35] (*continuous line*) and [37] (*long-dashed line*) are reported in the figure. Also shown is the relationship $(K_H/K_M)^{-1} = 1.0 + 3.7\overline{Ri_g}$ from [36] based on field experiments (*short-dashed line*)

dimensional) turbulent fluctuations. The dependence of statistical quantities on internal wave motions was investigated as well as how the turbulent kinetic energy is partitioned over a range of scales spanning from one to fifteen minutes. The results showed that the fraction of turbulent kinetic energy in pure turbulent motions compared to that of total motion field (turbulence and waves) decreases as the stability increases, from approximately 40 % when the gradient Richardson number $\overline{Ri_g} \cong 0.15$ to nearly 15 % for $\overline{Ri_g} \cong 1$.

The study also examined the applicability of MO similarity theory by analyzing the non-dimensional *rms* velocities σ_U/u_*, σ_V/u_* and σ_W/u_* (along-slope, cross-slope and slope-normal components, respectively) over a wide range of stabilities z/L, where L is the Obukhov scale.

For $z/L < 1$, (i) the MO similarity was reasonably applicable, with all normalized filtered and unfiltered *rms* velocities independent of z/L and (ii) the local scaling is applicable reasonably well, particularly for the vertical velocity component for both filtered and unfiltered data.

For stronger stability ($z/L > 1$), (i) the MO similarity was not applicable for both filtered and unfiltered data and (ii) the local scaling was not applicable for filtered and unfiltered

Author's personal copy

data for σ_U/u_*, (iii) local scaling is applicable for filtered data for σ_V/u_* and (iv) the local scaling worked well for σ_W/u_* for both filtered and unfiltered data.

Both σ_U/u_* and σ_V/u_* based on unfiltered data are greater than their filtered counterparts, irrespective of z/L. This is in contrast with the previous findings for nocturnal boundary layer over flat terrain under steady-state conditions (e.g. [7]), which showed a discrepancy between filtered and unfiltered data for the very stable regime only. This discrepancy may be attributed to active (critical) internal waves in complex terrain [1].

Estimates of momentum flux $\overline{u'w'}$ at $z = 13.9$ m as a function of $\overline{Ri_g}$ show that it changes the sign around $\overline{Ri_g} \approx 0.25$. A plausible explanation is the presence of low-level jets and their influence on the sign of computed momentum fluxes, but further direct measurements of local shear are needed to verify this conjecture.

Eddy diffusivities of momentum (K_M) and heat (K_H) showed an appreciable influence of wavy motions in the very stable regime, particularly at $z = 13.9$ m. The trend of the inverse turbulent Prandtl number $Pr^{-1} = K_H/K_M$ behavior with $\overline{Ri_g}$ broadly agrees with previous laboratory studies [35,37] as well as a field study [36], corroborating the growing evidence that $Pr \cong 1$ does not hold true for strongly stratified flows [39].

Acknowledgments The data analysis was performed with the support of Office of Naval Research Award # N00014-11-1-0709, Mountain Terrain Atmospheric Modeling and Observations (MATERHORN) Program.

References

1. Princevac M, Hunt JCR, Fernando HJS (2008) Quasi-steady katabatic winds over long slopes in wide valleys. J Atmos Sci 65(2):627–643
2. Whiteman CD (2000) Mountain meteorology: fundamentals and applications. Oxford University Press, Oxford
3. Fernando HJS (2010) Fluid dynamics of Urban atmospheres in complex terrain. Annu Rev Fluid Mech 42:365–389
4. Fernando HJS, Weil J (2010) An essay: whither the SBL? - A shift in the research agenda. B Am Meteorol Soc 91(11):1475–1484
5. Nieuwstadt FTM (1984) The turbulent structure of the stable, nocturnal boundary layer. J Atmos Sci 41:2202–2216
6. King JC (1990) Some measurements of turbulence over an Antarctic ice shelf. Q J Roy Meteor Soc 116:379–400
7. Mahrt L, Sun J, Jensen NO, Blumen W, Delany T, Oncley S (1998) Nocturnal boundary-layer regimes. Bound-Lay Meteorol 88:255–278
8. Van de Wiel BJH, Moene AF, Hartogensis OK, De Bruin HAR, Holtslag AAM (2003) Intermittent turbulence in the stable boundary layer over land. Part III: a classification for observations during CASES-99. J Atmos Sci 60:2509–2522
9. Van der Avoird E, Duynkerke PG (1999) Turbulence in a katabatic flow. Bound-Lay Meteorol 92:39–66
10. Munro DS, Davies JA (1978) On fitting the log-linear model to wind speed and temperature profiles over a melting glaciers. Bound-Lay Meteorol 15:423–437
11. Mahrt L (1998) Stratified atmospheric boundary layers and breakdown of models. Theoret Comput Fluid Dyn 11:263–279
12. Smedman AS (1988) Observations of a multi-level turbulence structure in a very stable atmospheric boundary layer. Bound-Lay Meteorol 44:231–253
13. Högström U (1990) Analysis of turbulent structures in the surface layer with a modified similarity formulation for near neutral conditions. J Atmos Sci 47:1949–1972
14. Monti P, Fernando HJS, Princevac M, Chan WC, Kowalewski TA, Pardyjak ER (2002) Observations of flow and turbulence in the nocturnal boundary layer over a slope. J Atmos Sci 59(17):2513–2534
15. DeSilva IPD, Imberger J, Ivey G (1997) Localized mixing due to a breaking internal wave ray at a sloping bed. J Fluid Mech 350:1–27
16. Bretherton FP (1969) Waves and turbulence in stably stratified fluids. Radio Sci 4(12):1279–1287

Author's personal copy

17. Finnigan J (1999) A note on wave-turbulence interaction and the possibility of scaling the very stable boundary layer. Bound-Lay Meteorol 90:529–539
18. Mahrt L, Vickers D, Sun J, Jensen NO, Jørgensen H, Pardyjak E, Fernando HJS (2001) Determination of the surface drag coefficient. Bound-Lay Meteorol 99:249–276
19. Doran JC, Fast JD, Horel J (2002) The VTMX 2000 campaign. B Am Meteorol Soc 83(4):537–554
20. Gibson CH (1980) Fossil temperature, salinity, and vorticity turbulence in the ocean. In: Nihoul J (ed) Marine Turbulence. Elsevier Publishing Co., Amsterdam, pp 221–257
21. McEwan AD (1983a) Internal mixing in stratified fluids. J Fluid Mech 128:59–80
22. McEwan AD (1983b) The kinematics of stratified mixing through internal wave breaking. J Fluid Mech 128:47–58
23. Fernando HJS (1991) Turbulent mixing in stratified fluids. Ann Rev Fluid Mech 23:455–493
24. Corral C (2000) Designing elliptic filters with maximum selectivity. In: Energy for the design mind (EDN), design feature, Motorola Inc, Schaumburg
25. Stull RB (1988) An introduction to boundary layer meteorology. Kluwer Academic Publisher, Dordrecht
26. Businger JA, Wyngaard JC, Izumi Y, Bradley EF (1971) Flux profile relationships in the atmospheric surface layer. J Atmos Sci 28:181–189
27. De Bruin HAR, Kohsiek W, van den Hurk JJM (1993) A verification of some methods to determine the fluxes of momentum, sensible heat, and water vapour using standard deviation and structure parameter of scalar meteorological quantities. Bound-Lay Meteorol 63:231–257
28. Pahlow M, Parlange MB, Porté-Agel F (2001) On monin-obukhov similarity theory in the stable atmospheric boundary layer. Bound-Lay Meteorol 99:225–248
29. Heinemann G (2004) Local similarity properties of the continuously turbulent stable boundary layer over Greenland. Bound-Lay Meteorol 112:283–305
30. Zardi D, Whiteman CD (2012) Chapter 2 in diurnal mountain wind systems. In: Chow FK, DeWekker SFJ, Snyder B (eds) Mountain weather research and forecasting. Springer, Berlin, pp 35–119
31. Moraes OLL, Acevedo OC, Da Silva R, Magnago R, Siquera AC (2004) Nocturnal surface-layer characteristics at the bottom of a valley. Bound-Lay Meteorol 112:159–177
32. Malhi YS (1995) The significance of the dual solutions for the heat fluxes measured by the temperature fluctuation method in stable conditions. Bound-Lay Meteorol 74:389–396
33. Rotter J, Fernando HJS, Kit E (2007) Evolution of a forced stratified mixing layer. Phys Fluids 19(065107): 1–10
34. Strang EJ, Fernando HJS (2001) Vertical mixing and transport through a stratified shear layer. J Phys Oceanogr 31:2026–2048
35. Strang EJ, Fernando HJS (2001) Entrainment and mixing in stratified shear flows. J Fluid Mech 428:349–386
36. Mahrt L, Vickers D (2003) Formulation of turbulent fluxes in the stable boundary layer. J Atmos Sci 60:2538–2548
37. Monti P, Querzoli G, Cenedese A, Piccinini S (2007), Mixing properties of a stably stratified parallel shear layer. Phys Fluids 19(085104): 1–9
38. Shumann U, Gerz T (1995) Turbulent mixing in stably stratified shear flows. J Appl Meteor 34:33–48
39. Lee SM, Giori W, Princevac M, Fernando HJS (2006) A new turbulent parameterization for the nocturnal PBL over complex terrain. Bound-Lay Meteorol 119:109–134